



Cite this: DOI: 10.1039/c6ee03554j

Received 7th December 2016,
Accepted 16th February 2017

DOI: 10.1039/c6ee03554j

rsc.li/ees

Unlocking the capacity of iodide for high-energy-density zinc/polyiodide and lithium/polyiodide redox flow batteries†

Guo-Ming Weng, Zhejun Li, Guangtao Cong, Yucun Zhou and Yi-Chun Lu*

Highly soluble iodide/triiodide (I^-/I_3^-) couples are one of the most promising redox-active species for high-energy-density electrochemical energy storage applications. However, to ensure high reversibility, only two-thirds of the iodide capacity is accessed and one-third of the iodide ions act as a complexing agent to stabilize the iodine (I_2), forming I_3^- (I_2I^-). Here, we exploit bromide ions (Br^-) as a complexing agent to stabilize the iodine, forming iodine–bromide ions (I_2Br^-), which frees up iodide ions and increases the capacity. Applying this strategy, we demonstrate a novel zinc/iodine–bromide battery to achieve an energy density of $101 \text{ W h L}_{\text{posolyte+negolyte}}^{-1}$ (or $202 \text{ W h L}_{\text{posolyte}}^{-1}$), which is the highest energy density achieved for aqueous flow batteries to date. This strategy can be further generalized to nonaqueous iodide-based batteries (*i.e.* lithium/polyiodide battery), offering new opportunities to improve high-energy iodide-based energy storage technologies.

Energy storage systems are a critical enabling factor for deploying unstable and intermittent renewable power sources such as solar and wind power sources.^{1–5} Redox flow batteries (RFBs) are one of the most promising technologies for storing the intermittent energy generated from renewable sources, owing to their design flexibility in decoupling energy and power.^{2,6,7} However, conventional flow batteries exhibit about 10-fold lower energy density compared to Li-ion batteries ($\text{LIB} > 250 \text{ W h L}^{-1}$).^{2,8–11} Developing high-energy-density RFBs can reduce the system footprint and storage size and expand their usage to both stationary and transportation applications.^{2,6,7}

Increasing the energy density of the RFBs can be achieved by increasing the numbers of electron involved in the half-cell reactions, the concentration of redox active species and the cell voltage.^{2,12} The energy density of the state-of-the-art all-vanadium redox flow battery (VRFB) has been improved significantly

Broader context

Redox flow batteries (RFBs) are one of the most promising technologies for grid-scale energy storage and electric vehicle applications, owing to their design flexibility in decoupling power and energy. However, broader application of conventional RFBs has been limited by their low energy density. Highly soluble iodide/triiodide (I^-/I_3^-) couples are one of the most promising redox-active species to enable high-energy-density flow batteries. However, to ensure high reversibility, one-third of the iodide ions act as a complexing agent to stabilize iodine (I_2) instead of contributing to useful capacity. In this work, we propose and demonstrate a new concept of exploiting bromide ions (more abundant and cheaper than iodide) as a complexing agent to ‘free-up’ the iodide ions thereby increasing the usable capacity of iodide without forming irreversible free iodine. This strategy can be further generalized to nonaqueous iodide-based batteries, offering new opportunities to improve high-energy iodide-based energy storage technologies.

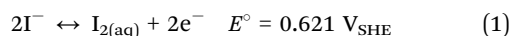
since it was first reported, but it remains unsatisfactory ($< 50 \text{ W h L}_{\text{posolyte+negolyte}}^{-1}$).^{10,13–15} In addition, the use of strong acids and the high cost of vanadium electrolytes is unavoidable in the VRFB.¹⁶ Currently, there is growing interest in employing water-soluble organic or polymer-based active species for aqueous RFBs, demonstrating energy densities around $10 \text{ W h L}_{\text{posolyte+negolyte}}^{-1}$.^{1,17} For practical applications, zinc-based aqueous hybrid flow batteries are on the verge of commercialization owing to their low cost and high performance.¹⁶ For instance, the zinc–bromine RFB is one of the practical alternatives because of its low cost and high energy density ($\sim 60 \text{ W h L}_{\text{posolyte+negolyte}}^{-1}$).^{8,16} Unfortunately, bromine is highly toxic and corrosive.^{8,18} A fully flowable Zn electrode was developed using semi-solid techniques to address the scalability limitation of Zn electrodes.¹⁹

Iodide has been identified as one of the most promising redox active species for redox flow batteries owing to its high solubility in both aqueous^{8,20} and nonaqueous media,¹² fast kinetics^{8,20,21} and high reversibility.^{8,20,21} For instance, in a Li–I aqueous flow battery system,²⁰ LiI has a high solubility of up to 8.2 M in water ($147 \text{ A h L}_{\text{posolyte}}^{-1}$), which is significantly higher than that in the conventional VRFBs ($\sim 2 \text{ M}$, $2.5 \text{ A h L}_{\text{posolyte+negolyte}}^{-1}$).^{22–24}

Electrochemical Energy and Interfaces Laboratory, Department of Mechanical and Automation Engineering, The Chinese University of Hong Kong, Shatin, N. T. 999077, Hong Kong SAR, China. E-mail: yichunlu@mae.cuhk.edu.hk

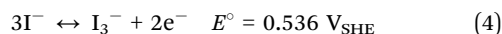
† Electronic supplementary information (ESI) available: Detailed experimental procedures and additional characterization. See DOI: 10.1039/c6ee03554j

In our recent work,¹² 5.0 M LiI was used to couple semi-solid sulfur-impregnated posolyte in a hybrid Li-nonaqueous redox flow battery yielding 550 A h L_{posolyte}^{-1} . Recently, Li *et al.*⁸ firstly reported a Zn-I flow battery (ZIB) using an ambipolar zinc iodide electrolyte with a maximum concentration of 5 M ZnI_2 . The concentration demonstrated is close to the saturation concentration reported by Shiloh *et al.* (5.6 M).²⁵ This novel system was demonstrated with both high power and superior energy density (167 W h L_{posolyte}^{-1}). The oxidation of iodide to iodine is often described in two steps *via* the formation of triiodide (I_3^-)^{26–28} (Standard potentials are calculated based on Table S1, see the ESI†)



The second reaction is an equilibrium reaction with a large equilibrium constant^{26,27} *i.e.*, the concentration of free iodine (I_2) is very low in the presence of excess iodide (I^-). The free iodine is stabilized by the iodide ion in the solution to form triiodide (eqn (2)). Upon further oxidation, the last one-third of the iodide is oxidized to I_2 (eqn (3)), where no free iodide is available to stabilize the iodine. Therefore, eqn (3) is often observed as being not as reversible as eqn (1).^{29–31} Due to the

low reversibility of reaction (3), the application of iodide as the redox active species in flow batteries has been limited in the first step,^{8,12,20} *i.e.* only 2/3 of the iodide ions contribute to the useable capacity and 1/3 of the iodide ions are used as a complexing agent to stabilize the free iodine (eqn (4)).



Here, we exploit bromide ions (Br^-) as the complexing agent to stabilize the free iodine forming iodine–bromide ions (I_2Br^-) as a means to free-up iodide ions for charge storage (Fig. 1a). While zinc chloride could also in principle be applied as a stabilization agent, it is known to exhibit severe hydrolysis issues.³² Therefore, bromide was selected to demonstrate this concept. The bromide ions were shown to stabilize iodine to form iodine–bromide (I_2Br^-).^{33,34} Both centrosymmetric I_3^- and asymmetric I_2Br^- have a linear (or nearly linear) trihalide structure³⁵ (Fig. 1b and c) and are thermodynamically stable.³⁶ In this approach, the cell voltage of ZIBB is purposely controlled to exclude the capacity contribution from the bromide/bromine couples (*e.g.* the equilibrium cell potential of zinc/bromine is 1.76 V) to avoid the formation of toxic and corrosive bromine. With this strategy, we here demonstrated a novel zinc/iodine–bromide (I_2Br^-) battery (ZIBB) with an energy density of 101 W h $L_{\text{posolyte+negolyte}}^{-1}$ (or 202 W h L_{posolyte}^{-1}), which is the highest energy density achieved experimentally for aqueous flow

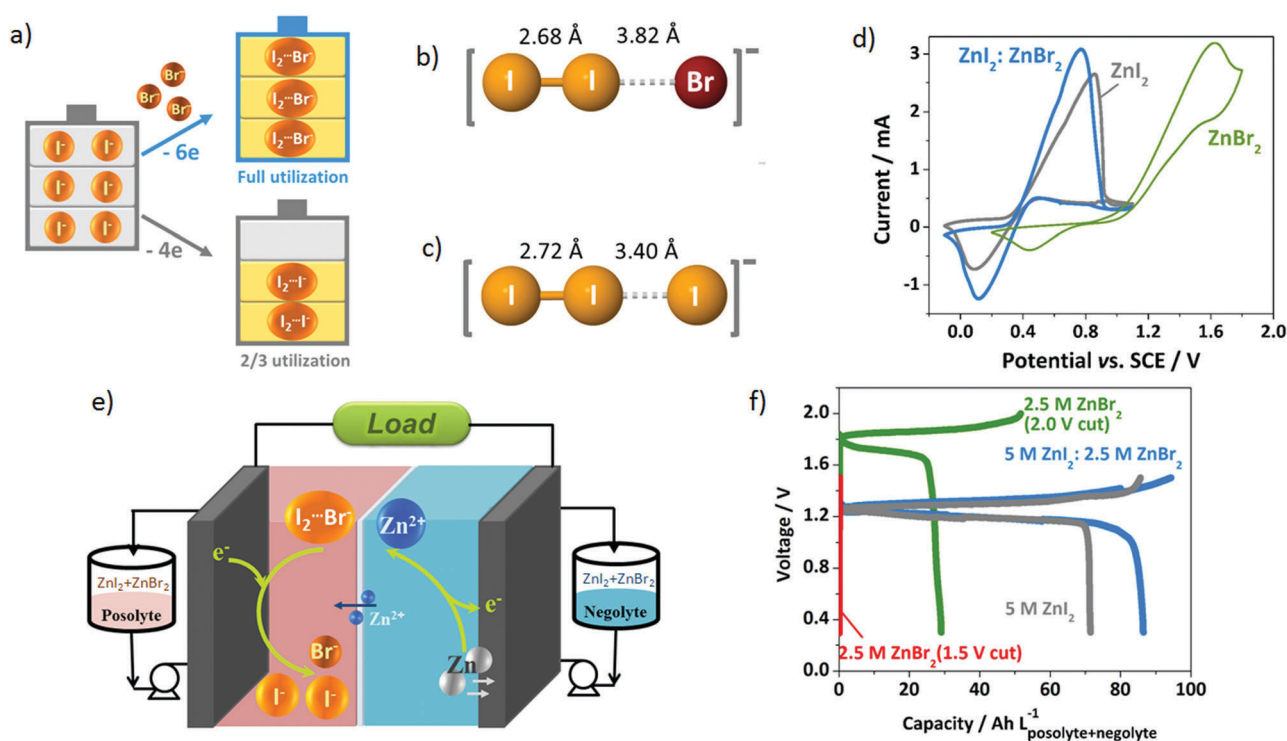
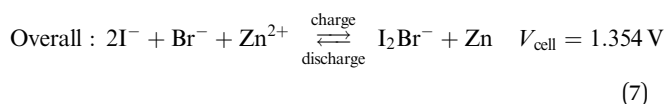
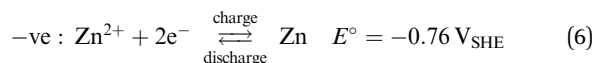
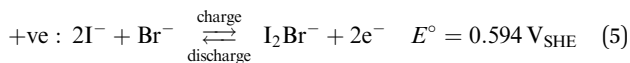


Fig. 1 (a) Concept illustration of bromide as the complexing agent to stabilize iodine. (b) Structure of the I_2Br^- ion. (c) Structure of the I_3^- ion. The bonding length of the polyhalide ion of zinc polyhalide is obtained from first-principles density functional theory calculations. (d) Cyclic voltammograms of 0.1 M ZnI_2 , 0.1 M $\text{ZnI}_2 + 0.05 \text{ M ZnBr}_2$ and 0.1 M $\text{ZnI}_2 + 0.1 \text{ M ZnBr}_2$ at a scan rate of 50 mV s^{-1} . (e) Schematic representation of the proposed ZIBB cell configuration. (f) Galvanostatic voltage profiles of the ZIBB systems with 5 M $\text{ZnI}_2 + 2.5 \text{ M ZnBr}_2$ as both posolyte and negolyte at a flow rate of 10 mL min^{-1} . The performance of the iodide-only system (5.0 M ZnI_2) under the same conditions is included. In addition, a bromide-only (2.5 M ZnBr_2) system with two cut off voltages, 1.5 V (red curve) and 2.0 V (green curve), is included for comparison. The charge/discharge current density is 5 mA cm^{-2} .

batteries to date. We examine the validity of this strategy using an electrospray ionization mass spectrometer (ESI-MS) to study the halide-containing species after oxidation of iodide in the presence of bromide ions. We further show that this strategy can be generalized in both aqueous and nonaqueous iodide-based redox flow batteries, offering new opportunities to further increase the energy density of aqueous and nonaqueous redox flow batteries.

We first investigate the influence of bromide ions on the redox behaviors and potential window of iodide using cyclic voltammetry. Fig. 1d shows the cyclic voltammogram (CV) of 0.1 M ZnI₂, 0.1 M ZnI₂ + 0.05 M ZnBr₂ and 0.1 M ZnBr₂ at the scan rate of 50 mV s⁻¹. The CV of bromide ions alone shows that the electrochemical oxidation potential of bromide ions (1.63 V vs. SCE, peak potential) is significantly higher than that of iodide oxidation (0.86 V vs. SCE, peak potential). That is, the oxidation of bromide (1.0–1.80 V vs. SCE) can be mostly excluded in the potential window of the oxidation of iodide (0.30–0.93 V vs. SCE). Water splitting is not observed in the positive potential region (*i.e.* oxygen evolution reaction, Fig. 1d) or in the negative potential region (hydrogen evolution reaction, Fig. S1, see ESI†). This is consistent with the water-stable electrochemical window for nearly neutral aqueous solutions (−1.7–1.2 V vs. SCE).⁸

We further evaluate how bromide ions influence the capacity of iodide polysolite in redox flow batteries. Fig. 1e shows the schematic representation of the proposed zinc/iodine–bromide redox flow battery (ZIBB) and Fig. S2 (see the ESI†) shows the photographs of a ZIBB single cell, which consists of a positive electrode of graphite felt (GF) operating in a mixed solution of ZnI₂ and ZnBr₂, Nafion membranes and a GF negative electrode in zinc polyhalide aqueous solution. The designed reactions of the ZIBB are shown in eqn (5)–(7), with a theoretical cell voltage similar to that of the zinc/iodide redox battery (ZIB), *ca.* 1.3 V.⁸ The theoretical standard electrode potential of the half-cell reaction shown in eqn (5) is determined to be 0.594 V based on the reported thermodynamic formation energy of each species³⁶ (Table S1, see the ESI†). Upon charging, I₂Br⁻ ions will be generated in the polysolite while the zinc ions are reduced to form zinc metal on the negative electrode. Such a process is accompanied by the movement of the zinc ions from the polysolite to negolyte serving as the charge carrier. Upon discharge, the reverse reactions occur.



While the solubility of ZnI₂ in water is quoted as 4500 g L_{H₂O}⁻¹, 7.0 M,⁸ we note that ZnI₂ precipitation starts to occur at concentrations larger than 5.5 M, as evidenced in Fig. S3 (see the ESI†),

showing the formation of solid precipitation at a concentration of 5.6 M ZnI₂. This observation is consistent with the saturation concentration reported by Shiloh *et al.*²⁵ (5.6 M ZnI₂) and the maximum demonstrated polysolite concentration by Li *et al.*⁸ (5.0 M ZnI₂). At concentrations larger than 5.0–5.5 M ZnI₂, we believe that partial or localized precipitation could occur during operation due to variation in the distribution of the active materials and/or water content in the flow cells. Fig. 1f compares the galvanostatic voltage profiles of a ZIBB (5.0 M ZnI₂:2.5 M ZnBr₂), and an iodide-only system (5.0 M ZnI₂) under continuous flow mode at 10 mL min⁻¹. In addition, a bromide-only (2.5 M ZnBr₂) system with two cut off voltages, 1.5 V (red curve) and 2.0 V (green curve), is included for comparison. Interestingly, with the same cut-off cell voltage (1.50 V), the cell with Br⁻ (ZIBB) achieves higher charge and discharge capacity compared with the iodide-only cell (ZIB). The bromide-only cell cut-off at 1.5 V shows no capacity and the bromide-only cell cut-off at 2.0 V shows an average voltage at ~1.8 V, which is consistent with the equilibrium voltage of zinc/bromine (1.76 V). These two control cells directly

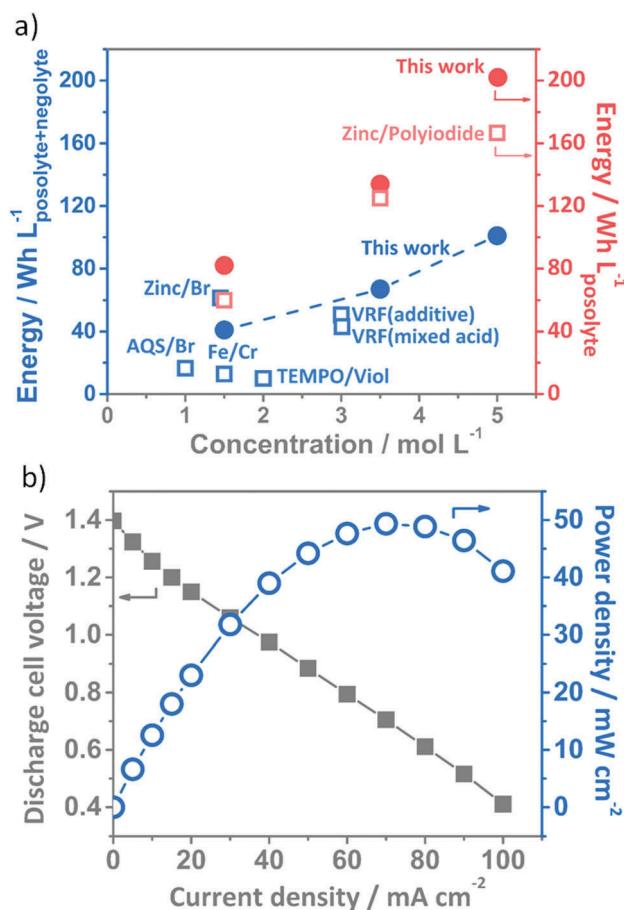


Fig. 2 (a) Comparison of the demonstrated energy density as a function of the concentration of active species for ZIBB and state-of-the-art aqueous flow batteries (AQS/Br,^{8,37} Fe/Cr,⁸ zinc/Br,^{8,16} TEMPO/Viol,¹ VRF (additive),¹⁴ VRF (mixed acid)¹⁵ and zinc/polyiodide⁸). The data of ZIBB were obtained from Fig. 1f and Fig. S5 (ESI†) (100% SOC). (b) Discharge polarization curves of the ZIBB with 3.5 M ZnI₂ + 1.75 M ZnBr₂ as both polysolite and negolyte at 10 mL min⁻¹ with one N-115.

demonstrate that the additional capacity observed in the ZIBB cell (cut at 1.5 V) does not originate from the oxidation of Br^- to Br_3^- . In addition, the enhanced capacity cannot be explained by the differences in the ionic conductivity since the ionic resistance of the ZIBB (5.0 M ZnI_2 :2.5 M ZnBr_2) is comparable to that of the iodide-only system (5.0 M ZnI_2) (Fig. S4, see the ESI†). We further evaluate the influence of the concentration of the active materials on the achievable capacity and energy density using three concentrations (X M ZnI_2 : $X/2$ M ZnBr_2 , where $X = 1.5, 3.5$ and 5.0). As shown in Fig. S5 (see the ESI†), the discharge capacity of the ZIBB with 1.5 M, 3.5 M and 5.0 M mixed electrolyte is *ca.* 32, 58, and 87 $\text{A h L}_{\text{posolyte+negolyte}}^{-1}$, respectively. By integrating the curve of voltage *vs.* capacity, the 1.5, 3.5, and 5.0 M ZIBB system yields a high energy density of 41, 67 and 101 $\text{W h L}_{\text{posolyte+negolyte}}^{-1}$, respectively (or 82, 134 and 202 $\text{W h L}_{\text{posolyte}}^{-1}$).

The demonstrated energy densities of the proposed ZIBB in continuous flow mode as a function of the electrolyte concentration are summarized and compared with other reported aqueous flow batteries (Fig. 2a). Depending on the availability of the reported value in the literature, two normalization bases for the energy density are used, including the energy density based on the volume of both posolyte and the negolyte ($\text{W h L}_{\text{posolyte+negolyte}}^{-1}$, left axis) as

well as the energy density based on the volume of the posolyte ($\text{W h L}_{\text{posolyte}}^{-1}$, right axis). The new ZIBB system proposed in this study exhibits the highest energy density among all reported aqueous redox flow batteries to date. Detailed calculations and comparison are summarized in Table S2 (see the ESI†). Fig. 2b shows the discharge polarization curve of a flow ZIBB (3.5 M ZnI_2 :1.75 M ZnBr_2) at 10 mL min^{-1} . The applied current densities range from 5 to 100 mA cm^{-2} . The highest power density achieved was 50 mW cm^{-2} at a current density of 70 mA cm^{-2} . The power density of the current prototype is mainly limited by Ohmic polarization with contact and ionic resistance associated with the membrane (Fig. S6, see the ESI†).

We then examine the cycling stability and the Coulombic efficiency of the proposed ZIBB flow battery. Fig. 3a and b show the galvanostatic cycling profiles of the 3.5 M and 5.0 M flow ZIBB system, respectively. The voltage profiles are stable over cycling with high capacity retention and Coulombic efficiency around 95%, as shown in Fig. 3c and d. Two Nafion N-117 membranes were used to prevent crossover at the expense of increased cell Ohmic resistance from 1.7Ω to 4.1Ω (Fig. S7, see the ESI†). To further quantify the contribution of voltage losses in the cell, we performed four-electrode measurements (Fig. S6, see the ESI†) during the operation of the ZIBB. We monitor the

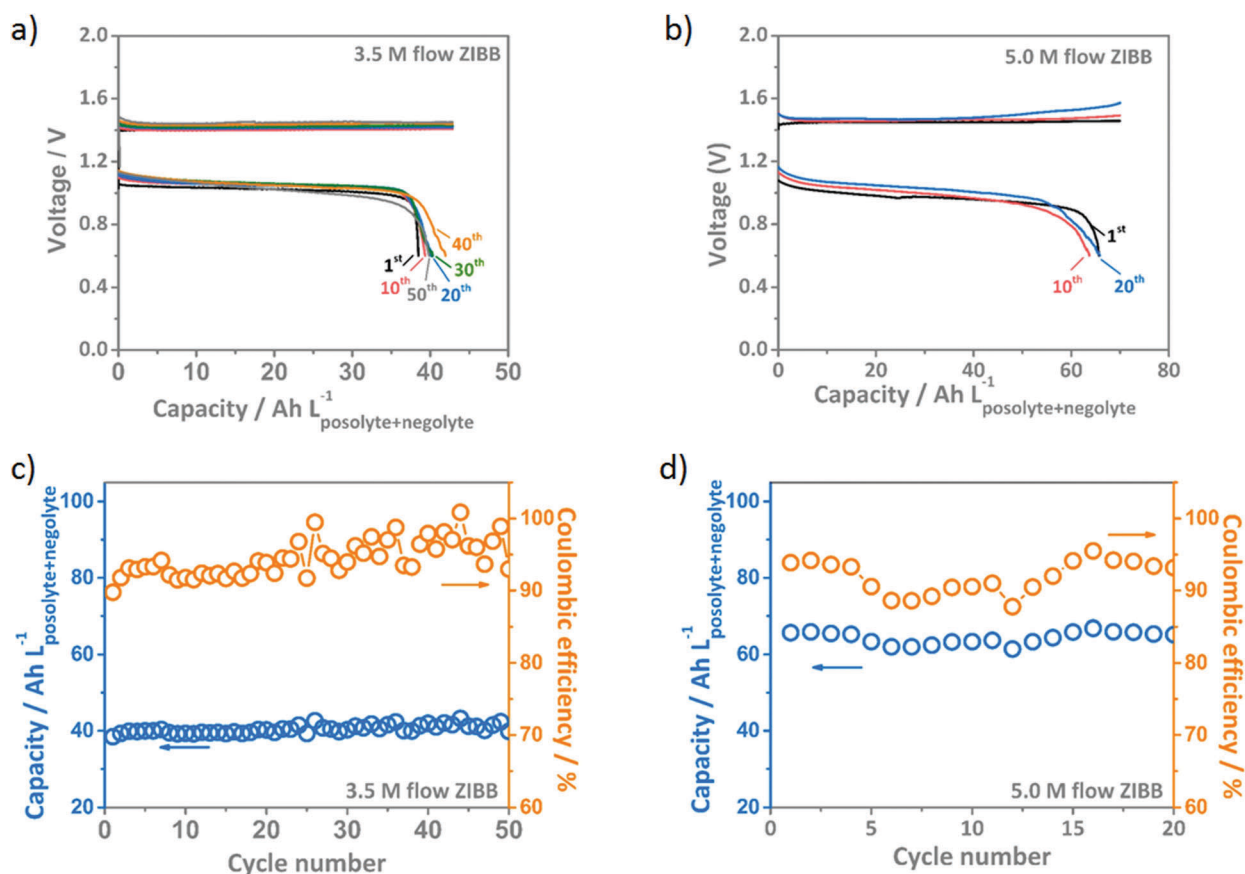
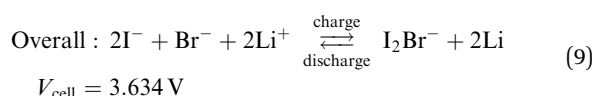
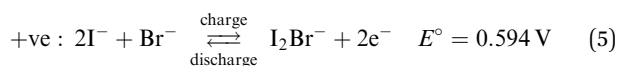


Fig. 3 Galvanostatic voltage profiles of (a) the ZIBB with 3.5 M ZnI_2 + 1.75 M ZnBr_2 as both posolyte and negolyte at 10 mL min^{-1} and (b) the ZIBB with 5 M ZnI_2 + 2.5 M ZnBr_2 as both posolyte and negolyte at 10 mL min^{-1} . Cycling retention in Coulombic efficiency and discharge capacity of (c) the ZIBB shown in (a), and (d) the ZIBB shown in (b). The charge/discharge current density is 10 mA cm^{-2} . Both systems are operated at a state-of-charge (SOC) of $\sim 70\%$.

voltage drop between the positive electrode and the SCE inserted in the posolyte (E_p), between the negative electrode and the SCE inserted in the negolyte (E_n), between the two SCE reference electrodes across the membrane (V_m), and between the positive and negative electrodes (V_{cell}). As shown in Fig. S6 (ESI[†]), the polarization during operation under 15 mA cm^{-2} at the positive side (ΔE_p) and the negative side (ΔE_n) is *ca.* 60 mV and 20 mV, respectively. These voltage losses in the positive electrode and negative electrode are much lower than the voltage loss across the membrane (*i.e.* $\Delta E_m = 220 \text{ mV}$, Fig. S6, ESI[†]), suggesting that the resistance of the ion-exchange membrane is the limiting factor of the ZIBB system and requires further development of the ion-exchange membrane for redox flow batteries.^{38–41}

We further demonstrate that this concept can be applied to halide systems in nonaqueous media for high-energy lithium storage, forming a lithium/iodine–bromide (I_2Br^-) battery (LIBB). Similarly, the negative and overall reactions of the LIBB are shown in eqn (8) and (9). The design cell reactions have a theoretical cell voltage of 3.634 V, which is similar to the lithium/iodide (aqueous) battery ($3.536 \text{ V vs. Li/Li}^+$)²⁰



We note that the observed reaction potentials of the halide redox are lower in nonaqueous electrolytes than that in aqueous electrolytes. For instance, the reaction potential of I^-/I_3^- redox in tetrahydrofuran (THF),⁴² carbonate-based solvents³¹ and 1,3-dioxolane (DOL):1,2-dimethoxyethane (DME) (1:1 v:v)¹² is *ca.* 3.0 V *vs.* Li/Li^+ , which is lower than that obtained in aqueous media ($3.536 \text{ V vs. Li/Li}^+$).²⁰ We construct LIBB single cells using a mixed nonaqueous solution of LiI and LiBr in 0.2 M LiClO_4 –0.1 M LiNO_3 in DOL:DME (1:1 v:v). To prevent crossover of active species, the posolyte and negolyte are separated by a lithium conductive $\text{Li}_{1.5}\text{Al}_{0.5}\text{Ge}_{1.5}(\text{PO}_4)_3$ (LAGP) ceramic membrane⁴³ (Fig. S8 (see the ESI[†])). Fig. 4a compares the galvanostatic voltage profiles of a LIBB (2.5 M LiI:1.25 M LiBr) and an iodide-only system (2.5 M LiI). Interestingly, with the same cut-off cell voltage (3.20 V), the cell with Br^- achieves higher charge and discharge capacity compared to the iodide-only cell. Since the cut-off voltage is significantly lower than the theoretical cell voltage of Li/bromine (4.01 V),¹⁸ we attribute the additional capacity to the iodide ions that are released from being complexing agents thanks to the presence of Br^- , which can be used to stabilize iodine (I_2) to form I_2Br^- , similar to the case shown in aqueous media (Fig. 1f). The LIBB shows exceptional stability with superior coulombic efficiency ($\sim 99\%$) and energy efficiency ($\sim 88\%$) over prolonged cycling at 100% SOC (Fig. 4b). This suggests that the concept of complexing iodine with free bromide ions to form iodine–bromide

(I_2Br^-) could be applied in both aqueous and nonaqueous environments, which offers new design strategies for high-energy iodide-based energy storage applications. The effect of bromide-stabilization is realized in both a nonaqueous LIBB and an aqueous ZIBB. We note that the LIBB showed higher stable cycling stability but lower power capability compared to the ZIBB, owing to the solid-state Li-ion conducting electrolyte (LAGP), which effectively blocks the crossover of active species but increases the Ohmic resistance. We believe that developing effective ion-exchange membranes is critical to further improving the stability and efficiency of the ZIBB.

To understand the origin of the additional capacity, we conducted ESI-MS to investigate the halide-containing ions after oxidation of the posolyte. As shown in Fig. 5a, I^- ($m/z = 126.9$) was identified in the initial ZIBB posolyte as expected. Trace amounts of I_2Br^- and I_3^- were observed in the initial ZIBB posolyte, which could be related to the formation of trace amounts of iodine present in aqueous iodide solution.⁴⁴ Comparatively, the relative amount of I_2Br^- ($m/z = 333.7$), and I_3^- ($m/z = 380.7$), together with

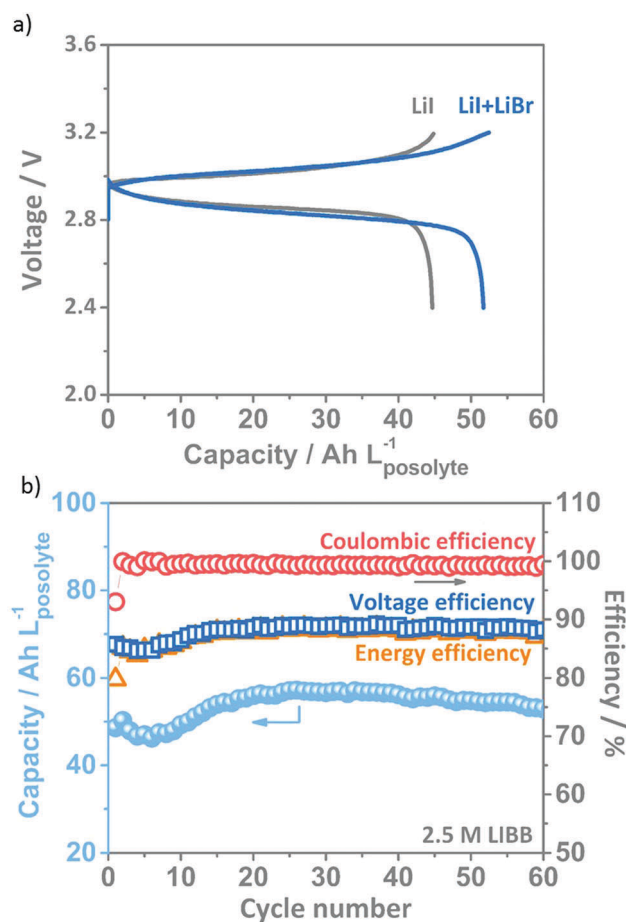


Fig. 4 (a) Galvanostatic voltage profiles of the LIBB system with 2.5 M LiI + 1.25 M LiBr as posolyte. A controlled system using 2.5 M LiI as posolyte is included for comparison. The charge/discharge current density is 0.1 mA cm^{-2} . (b) Cycling retention in efficiency and discharge capacity of the LIBB system with 2.5 M LiI + 1.25 M LiBr as posolyte. The charge/discharge current density is 0.44 mA cm^{-2} . Both tests are operated at a state-of-charge (SOC) of 100%.

$[\text{ZnI}_2\text{Br}]^-$ ($m/z = 399.1$) and $[\text{ZnI}_3]^-$ ($m/z = 446.1$) clusters increased after the oxidation in the ZIBB cell. The formation of cluster ions $[\text{M}_n\text{X}_m]^-$ in ESI-MS is well-documented in previous reports.^{27,45,46} Combining the ESI-MS results and the additional capacity observed in the electrochemical cell (Fig. 1f), we believe that the Br^- complexes with the free iodine in the oxidized ZIBB posolyte.

In contrast, in an iodide-only ZIB system,⁸ a dominant peak associated with I_3^- ($m/z = 380.7$) was observed.⁸ We further conducted ESI-MS to investigate the halide-containing ions in the nonaqueous media after fully charging (SOC 100%) the LIBB posolyte. As shown in Fig. 5b, the ESI-MS results unambiguously identify the presence of I_2Br^- ($m/z = 333.7$) after oxidation in the LIBB cell, compared to the initial posolyte. In addition, the ESI-MS results of the ZIBB and LIBB showed that

no Br_3^- ($m/z = 239.7$) ion species were found in the charged posolyte. This evidence together with Fig. 1f directly confirms that no capacity contribution from the $\text{Br}^-/\text{Br}_3^-$ redox couple took place. Other ESI-MS peaks observed in the posolyte can be attributed to the common anionic cluster derivatives of zinc ions^{27,47} and solvation,^{48,49} which are listed in detail in the figure captions. These observations confirm that the bromide ions act as complexing agents to the iodine, in which case some iodide ions become available for storing charge, which could contribute to the additional capacity compared to the pure iodide-system.

Conclusions

In summary, we employ bromide ions (Br^-) as the complexing agent to stabilize free iodine and form iodine–bromide ions (I_2Br^-), thereby increasing the capacity of the iodide ions. We first show that the capacity of iodide can be increased in the presence of Br^- ions without involving redox reactions of $\text{Br}^-/\text{Br}_3^-$. With this strategy, we demonstrate a novel zinc/iodine–bromide (I_2Br^-) battery (ZIBB) achieving an energy density of $101 \text{ W h L}_{\text{posolyte+negolyte}}^{-1}$ (or $202 \text{ W h L}_{\text{posolyte}}^{-1}$), which is the highest energy density achieved for aqueous flow batteries to date. ESI-MS measurements identify the presence of the iodine–bromide ions (I_2Br^-) of the posolytes after the oxidation in the ZIBB/LIBB, supporting that the Br^- ions serve as complexing agents to stabilize iodine ions. Our strategy enables high-energy-density redox chemistry with stable cyclability and high efficiencies, and can be generalized to nonaqueous media, offering new opportunities to improve high-energy iodide-based energy storage technologies.

Acknowledgements

This work is supported by a grant from the Research Grants Council (RGC) of the Hong Kong Administrative Region, China, under Theme-based Research Scheme through project no. T23-407/13-N, a RGC project No. CUHK14200615 and a grant from the Innovation and Technology Commission of Hong Kong Special Administrative Region, China (Project No. ITS/248/14FP). The authors are grateful to Mr Long-Yin Simon Tam at The Chinese University of Hong Kong for assisting with the flow battery test.

Notes and references

- 1 T. Janoschka, N. Martin, U. Martin, C. Friebe, S. Morgenstern, H. Hiller, M. D. Hager and U. S. Schubert, *Nature*, 2015, **527**, 78–81.
- 2 G. L. Soloveichik, *Chem. Rev.*, 2015, **115**, 11533–11558.
- 3 J. Lu, Y. J. Lee, X. Luo, K. C. Lau, M. Asadi, H.-H. Wang, S. Brombosz, J. Wen, D. Zhai and Z. Chen, *Nature*, 2016, **529**, 377–382.
- 4 V. Amstutz, K. E. Toghill, F. Powlesland, H. Vrubel, C. Comninellis, X. Hu and H. H. Girault, *Energy Environ. Sci.*, 2014, **7**, 2350–2358.

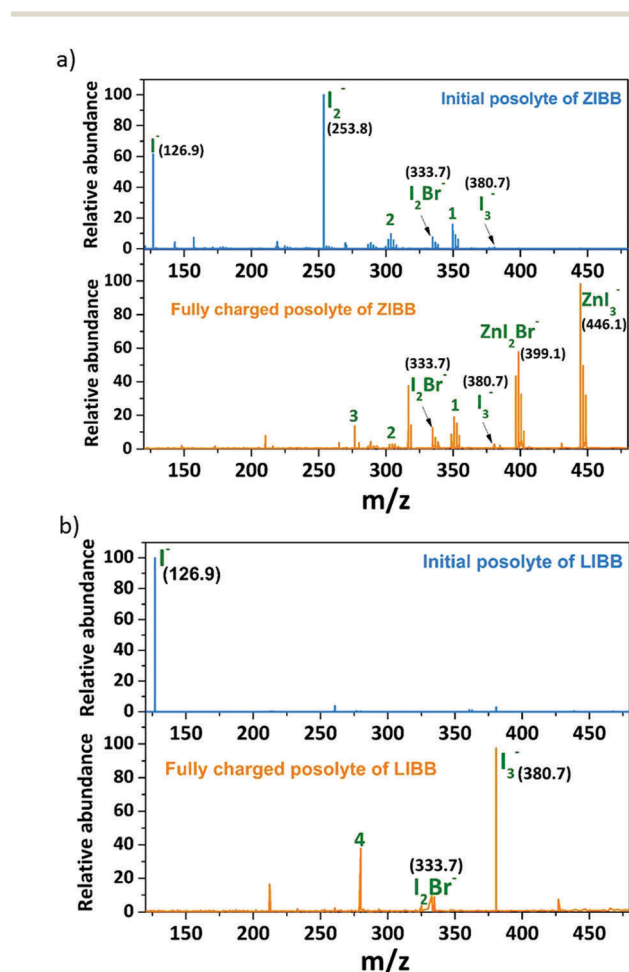


Fig. 5 (a) ESI-MS of the fully charged ZIBB posolyte (5 M ZnI_2 + 2.5 M ZnBr_2). Initial electrolyte was also included for comparison. (b) ESI-MS of the fully charged LIBB posolyte (2.5 M LiI + 1.25 M LiBr). Initial electrolyte was also included for comparison. The peaks located at $m/z = 446.1$ and $m/z = 399.1$ are assigned to zincate ions ZnI_3^- and ZnI_2Br^- respectively thanks to their isotopic pattern.⁴⁷ The peaks 1, 2, 3 and 4 could be assigned to the species or their relative isotopes of $\text{ZnI}_2\text{Br}_2^-$, ZnBr_3^- , $\text{IBr}(\text{H}_2\text{O})^-$ and $\text{IBr}(\text{DMF})^-$, respectively. The peak intensity may not represent the respective ion concentration in the electrolyte because the tested solution is diluted (ZIBB posolyte: by H_2O , LIBB posolyte: by DMF) about 100 000 times to obtain high resolution spectra⁸ and ESI-MS does not allow any quantification of these equilibria.²⁷

- 5 Y. Ding, Y. Zhao, Y. Li, J. B. Goodenough and G. Yu, *Energy Environ. Sci.*, 2017, **10**, 491–497.
- 6 T. V. Nguyen and R. F. Savinell, *Electrochem. Soc. Interface*, 2010, **19**, 54–56.
- 7 A. Z. Weber, M. M. Mench, J. P. Meyers, P. N. Ross, J. T. Gostick and Q. Liu, *J. Appl. Electrochem.*, 2011, **41**, 1137–1164.
- 8 B. Li, Z. Nie, M. Vijayakumar, G. Li, J. Liu, V. Sprenkle and W. Wang, *Nat. Commun.*, 2015, **6**, 6303.
- 9 X. Zhou, H. Xu, J. Cheng, N. Zhao and S.-C. Chen, *Sci. Rep.*, 2015, **5**, 10402.
- 10 K. Lin, R. Gómez-Bombarelli, E. S. Beh, L. Tong, Q. Chen, A. Valle, A. Aspuru-Guzik, M. J. Aziz and R. G. Gordon, *Nat. Energy*, 2016, **1**, 16102.
- 11 Y. Zhao, Y. Ding, Y. Li, L. Peng, H. R. Byon, J. B. Goodenough and G. Yu, *Chem. Soc. Rev.*, 2015, **44**, 7968–7996.
- 12 H. Chen and Y. C. Lu, *Adv. Energy Mater.*, 2016, 1502183.
- 13 L. Li, S. Kim, W. Wang, M. Vijayakumar, Z. Nie, B. Chen, J. Zhang, G. Xia, J. Hu and G. Graff, *Adv. Energy Mater.*, 2011, **1**, 394–400.
- 14 S. Roe, C. Menictas and M. Skyllas-Kazacos, *J. Electrochem. Soc.*, 2016, **163**, A5023–A5028.
- 15 Y. Zeng, T. Zhao, L. An, X. Zhou and L. Wei, *J. Power Sources*, 2015, **300**, 438–443.
- 16 P. Leung, X. Li, C. P. De León, L. Berlouis, C. J. Low and F. C. Walsh, *RSC Adv.*, 2012, **2**, 10125–10156.
- 17 J. Winsberg, T. Janoschka, S. Morgenstern, T. Hagemann, S. Muench, G. Hauffman, J. Gohy, M. D. Hager and U. S. Schubert, *Adv. Mater.*, 2016, 201505000.
- 18 P. Bai and M. Z. Bazant, *Electrochim. Acta*, 2016, **202**, 216–223.
- 19 J. Liu and Y. Wang, *J. Power Sources*, 2015, **294**, 574–579.
- 20 Y. Zhao, L. Wang and H. R. Byon, *Nat. Commun.*, 2013, **4**, 1896.
- 21 Z. Li, G. Weng, Q. Zou, G. Cong and Y.-C. Lu, *Nano Energy*, 2016, **30**, 283–292.
- 22 H. Chen, Q. Zou, Z. Liang, H. Liu, Q. Li and Y.-C. Lu, *Nat. Commun.*, 2015, **6**, 5877.
- 23 G. M. Weng, C. Y. V. Li, K. Y. Chan, C. W. Lee and J. Zhong, *J. Electrochem. Soc.*, 2016, **163**, A5180–A5187.
- 24 K. Gong, X. Ma, K. M. Conforti, K. J. Kuttler, J. B. Grunewald, K. L. Yeager, M. Z. Bazant, S. Gu and Y. Yan, *Energy Environ. Sci.*, 2015, **8**, 2941–2945.
- 25 M. Shiloh, M. Givon and Y. Marcus, *J. Inorg. Nucl. Chem.*, 1969, **31**, 1807–1814.
- 26 M. Davies and E. Gwynne, *J. Am. Chem. Soc.*, 1952, **74**, 2748–2752.
- 27 J. S. McIndoe and D. G. Tuck, *Dalton Trans.*, 2003, 244–248.
- 28 J. C. Verhoef and E. Barendrecht, *Electrochim. Acta*, 1978, **23**, 433–438.
- 29 E. C. Toren Jr and C. P. Driscoll, *Anal. Chem.*, 1966, **38**, 872–876.
- 30 R. Osteryoung and F. Anson, *Anal. Chem.*, 1964, **36**, 975–980.
- 31 Y. Wang, Q. Sun, Q. Zhao, J. Cao and S. Ye, *Energy Environ. Sci.*, 2011, **4**, 3947–3950.
- 32 B. V. R. Narayan, *Chemical And Electrochemical Energy Systems*, 1998.
- 33 V. K. L. Mer and M. H. Lewinsohn, *J. Phys. Chem.*, 1933, **38**, 171–195.
- 34 D. Meyerstein and A. Treinin, *Trans. Faraday Soc.*, 1963, **59**, 1114–1120.
- 35 M. C. Aragoni, M. Arca, F. A. Devillanova, M. B. Hursthouse, S. L. Huth, F. Isaia, V. Lippolis, A. Mancini, H. R. Ogilvie and G. Verani, *J. Organomet. Chem.*, 2005, **690**, 1923–1934.
- 36 A. J. Bard, R. Parsons and J. Jordan, *Standard potentials in aqueous solution*, CRC Press, 1985.
- 37 Q. Chen, M. R. Gerhardt, L. Hartle and M. J. Aziz, *J. Electrochem. Soc.*, 2016, **163**, A5010–A5013.
- 38 J. R. Varcoe, P. Atanassov, D. R. Dekel, A. M. Herring, M. A. Hickner, P. A. Kohl, A. R. Kucernak, W. E. Mustain, K. Nijmeijer and K. Scott, *Energy Environ. Sci.*, 2014, **7**, 3135–3191.
- 39 W. Wang, Q. Luo, B. Li, X. Wei, L. Li and Z. Yang, *Adv. Funct. Mater.*, 2013, **23**, 970–986.
- 40 C. Ding, H. Zhang, X. Li, T. Liu and F. Xing, *J. Phys. Chem. Lett.*, 2013, **4**, 1281–1294.
- 41 L. Zeng, T. Zhao, L. An, G. Zhao and X. Yan, *Energy Environ. Sci.*, 2015, **8**, 2768–2774.
- 42 W. K. Behl and D. T. Chin, *J. Electrochem. Soc.*, 1988, **135**, 16–21.
- 43 H. Kitaura and H. Zhou, *Energy Environ. Sci.*, 2012, **5**, 9077–9084.
- 44 E. Kendall, *J. Biol. Chem.*, 1920, **43**, 19.
- 45 J. Anacleto, S. Pleasance and R. Boyd, *Org. Mass Spectrom.*, 1992, **27**, 660–666.
- 46 C. Hasselgren, K. Fisher, S. Jagner and I. Dance, *Chem. – Eur. J.*, 2000, **6**, 3671–3678.
- 47 K. Koszinowski and P. Böhrer, *Organometallics*, 2009, **28**, 771–779.
- 48 H. Wakita, G. Johansson, M. Sandström, P. L. Goggin and H. Ohtaki, *J. Solution Chem.*, 1991, **20**, 643–668.
- 49 E. Kálmán, I. Serke, G. Pálinkás, G. Johansson, G. Kabisch, M. Maeda and H. Ohtaki, *Z. Naturforsch., A: Phys., Phys. Chem., Kosmophys.*, 1983, **38**, 225–230.